PROCEEDINGS A

Research

CrossMark
click for updates

Classical homogenization to analyse the dispersion relations of spoof plasmons with geometrical and compositional effects

J. -F. Mercier[1], M. L. Cordero[2], S. Félix[3], A. Ourir[4] and A. Maurel[4]

[1] Poems, ENSTA ParisTech, CNRS, Inria, Université Paris-Sachay, 828 boulevard des Maréchaux, Palaiseau cedex, 91762, France
[2] Departamento de Física Facultad de Ciencias Físicas y Matemáticas, Universidad de Chile Av. Blanco Encalada, Santiago 2008, Chile
[3] LAUM, CNRS, Université du Maine, avenue Olivier Messiaen, Le Mans 72085, France
[4] Institut Langevin, CNRS, ESPCI ParisTech, 1 rue Jussieu, Paris 75005, France

We show that the classical homogenization is able to describe the dispersion relation of spoof plasmons in structured thick interfaces with periodic unit cell being at the subwavelength scale. This is because the interface in the real problem is replaced by a slab of an homogeneous birefringent medium, with an effective mass density tensor and an effective bulk modulus. Thus, explicit dispersion relation can be derived, corresponding to guided waves in the homogenized problem. Contrary to previous effective medium theories or retrieval methods, the homogenization gives effective parameters depending only on the properties of the material and on the geometry of the microstructure. Although resonances in the unit cell cannot be accounted for within this low-frequency homogenization, it is able to account for resonances occurring because of the thickness of the interface and thus, to capture the behaviour of the spoof plasmons. Beyond the case of simple grooves in a hard material, we inspect the influence of tilting the grooves and the influence of the material properties.

THE ROYAL SOCIETY
PUBLISHING

1. Introduction

Man-made materials designed to control the propagation of waves are based on the observation of the properties of natural materials, transposed to a larger scale. Photonic and phononic artificial crystals are inspired from atomic lattices able to forbid the propagation of electrons. These artificial crystals produce a strong coupling with the wave able to realize wave guiding and light slowing [1–3] and to produce resonant ultra-directional sources, optical fibres and bio-sensors [4–7]. Nevertheless, being associated to the band structure of the periodic medium, they have two major drawbacks: they have a wavelength scale period that cannot be reduced and they are inherently sensitive to any weakening in the constructive or destructive interferences, such as the weakening due to the attenuation or to the disorder [8,9].

Alternatively to artificial crystals, metamaterials built with a subwavelength unit cell behave as homogeneous materials at large scale, with effective properties being, in general, anisotropic. This artificial anisotropy can be engineered by assigning a desired value of each parameter of the permeability and/or permittivity tensors [10–12]. To that aim, at least two theoretical ingredients have nowadays reached a level of sophistication that can be leveraged for the design of unique manufacturable optical components (i) geometrical, or optical, transformations provide in a mathematically rigorous formalism the permeability and permittivity tensors of the metamaterial able to control the wave propagation in a proper way [13], (ii) retrieval methods [14,15] or homogenization theories [16–20] allow to design the unit cell restituting the desired effective tensors at large scale.

In this paper, we use a formalism based on the effective anisotropy able to give a simple and comprehensive picture of the resonances that can take place in such metamaterials, and which are not related to the resonances of constituents in the unit cell; the reader interested by high-frequency homogenization may refer to, for example, [21] and references herein. Our formalism captures the dispersion relation of guided waves (being guided within the homogenized slab) which corresponds to the dispersion relation of plasmons and spoof plasmons in the actual metamaterial.

The wave equation is written for a two-dimensional problem in a generic form

$$\nabla \cdot [a\nabla p(x,y)] + k^2 b p(x,y) = 0, \tag{1.1}$$

where a and b are relative parameters measured with respect to a reference medium (where $a = 1$, $b = 1$), and k the wavenumber in the reference medium. A time dependence $e^{-i\omega t}$ is assumed and it is omitted in the following. This equation applies for acoustic waves

$$\nabla \cdot \left[\frac{1}{\rho}\nabla p(x,y)\right] + \frac{k^2}{B} p(x,y) = 0, \tag{1.2}$$

with p the pressure field, (ρ, B) the mass density and bulk modulus, respectively. For electromagnetic waves, we restrict ourselves to the case of transverse magnetic polarization (the magnetic field $\mathbf{H} = H(x,y)\mathbf{e_z}$ is perpendicular to the incidence plane), leading to

$$\nabla \cdot \left[\frac{1}{\varepsilon}\nabla H(x,y)\right] + k^2 \mu H(x,y) = 0, \tag{1.3}$$

with (ε, μ) the permittivity and permeability, respectively. The same structure of the wave equation can be found for a transverse electric field as for elastic simple harmonic waves or water waves.

The paper is organized as follows. In §2, we derive the dispersion relation of waves guided in a homogeneous isotropic slab surrounded by air for acoustics or vacuum for electromagnetism (the reference medium hereafter referred as medium Ⓐ) and by a substrate (hereafter referred as medium Ⓒ). The derivation is done in an unusual way by solving a scattering problem, rather than solving a homogeneous problem, and the equivalence between the two derivations

is provided. It allows the characterization of the behaviour of the slab for waves being either propagating or evanescent in the succession of media. The approach is then generalized to the case of a homogeneous anisotropic slab, and the place where guided waves can take place are given, as their associated dispersion relations.

In §3, the homogenization theory of layered media is briefly recalled, which provides a rigorous mathematical formalism to get the effective parameters of a microstructured interface (we restricted ourselves to the case of periodic layers, with period d, being possibly tilted). Next, the equivalence between the scattering properties of this structured interface and the homogenized anisotropic slab is inspected and discussed in terms of the periodicity value, that has been assumed to be small in the homogenization process (typically, the homogenization is found to be robust for kd values up to about 0.3).

Practical illustrations are given in §4 for gratings and arrays (called sometimes 'Reflection gratings' and 'Transmission gratings'). In the context of electromagnetic waves, we recover the dispersion relation for Neumann structured grating (spoof plasmons [17–19]); the case of an array (structured interface in air) is also regarded. In the context of acoustics, we study the impact of the variations of the physical characteristics of the layer material on the properties of the guided waves, and we show that a significant tuning is achievable.

2. The problem of guided waves by a homogeneous slab: the isotropic and anisotropic case

The propagation of waves in an anisotropic medium is described by

$$\nabla . [\mathsf{a}\nabla p(x,y)] + k^2 b p(x,y) = 0, \tag{2.1}$$

with $p_{\text{inc}}(x,y)$ an incident wave, where a is a tensor, which reduces to $\mathsf{a} = a\mathsf{I}$ for isotropic media (and I is the identity). In the principal directions of anisotropy (X,Y), a is diagonal and it is denoted

$$\mathsf{a} = \begin{pmatrix} a_{\text{e}} & 0 \\ 0 & a_{\text{o}} \end{pmatrix}_{(X,Y)}. \tag{2.2}$$

As for a birefringent medium, we associate the direction X to the extraordinary refractive index n_{e} and the direction Y to the ordinary refractive index n_{o}, with

$$n_{\text{e}} \equiv \sqrt{\frac{b}{a_{\text{e}}}} \quad \text{and} \quad n_{\text{o}} \equiv \sqrt{\frac{b}{a_{\text{o}}}}. \tag{2.3}$$

In this section, we recall the derivation of the dispersion relation of classical guided waves within an homogeneous slab, being isotropic or anisotropic (ⓑ being homogeneous, figure 1). A guided wave corresponds to a resonant wave, propagating along x within the slab and evanescent when moving away from the slab, along the y-direction ($p(x, |y| \to \infty) \to 0$). Classically, guided waves $p_{\text{hom}}(x,y)$ are found by solving the homogeneous problem (without incident wave) with $p_{\text{hom}}(x, |y| \to \infty) = 0$ which leads to solve an eigenvalue problem [22] where k^2 plays the role of the eigenvalue. When such a wave exits (say, at certain frequencies), the scattering problem (that is in the presence of an incident wave) is ill posed. The non-inversibility of the wave operator is due to the existence of solutions of the homogeneous problem and thus to the non-uniqueness of the solution. If one insists in solving the scattering problem, as we do in the following, a divergence of the scattering coefficients at these frequencies is observed. Note that this divergence of the scattering coefficients does not question the energy conservation since the incident wave will be found evanescent, and thus, does not transport energy.
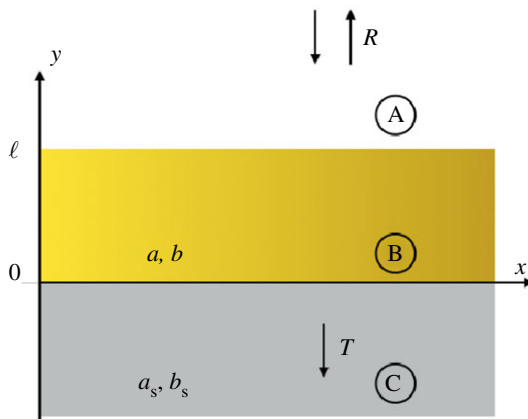
Figure 1. Scattering problem by a homogeneous isotropic slab Ⓑ of thickness ℓ between air Ⓐ and a substrate Ⓒ. The slab material is characterized by the two scalars a and b. (Online version in colour.)

(a) Classical guided waves in a homogeneous isotropic waveguide

A guided wave is a non-zero solution of (2.1) in the form

$$
\left.
\begin{aligned}
p(x, y \geq \ell) &= e^{ik_x x} r\, e^{i\sqrt{k^2 - k_x^2}\, y}, \\
p(x, 0 < y \leq \ell) &= e^{ik_x x}\left[m^- e^{-i\sqrt{n^2 k^2 - k_x^2}\, y} + m^+ e^{i\sqrt{n^2 k^2 - k_x^2}\, y}\right]
\end{aligned}
\right\}
\tag{2.4}
$$

and
$$
p(x, y \leq 0) = e^{ik_x x} t\, e^{-i\sqrt{n_s^2 k^2 - k_x^2}\, y},
$$

with the refractive indices $n^2 = b/a$ in the medium Ⓑ and $n_s^2 = b_s/a_s$ in the medium Ⓒ ($a = b = 1$ in the medium Ⓐ). Such guided wave exists only along the dispersion relation $k_x = \beta(k)$ we are looking for. In practice, it is easier to look for a scattered solution since the scattering problem by a homogeneous isotropic slab (figure 1) is a trivial one-dimensional problem (along y). We denote x the direction along the slab and y the transverse direction.

With an incident wave of the form

$$
p^{\text{inc}}(x, y) = P^{\text{inc}} e^{ik_x x - i\sqrt{k^2 - k_x^2}\, y}
\tag{2.5}
$$

(and P^{inc} is not unity for convenience), the wavefield solution of equations (1.1) is

$$
\left.
\begin{aligned}
p(x, y \geq \ell) &= e^{ik_x x} P^{\text{inc}}[e^{-i\sqrt{k^2 - k_x^2}\, y} + R\, e^{i\sqrt{k^2 - k_x^2}\, y}], \\
p(x, 0 < y \leq \ell) &= e^{ik_x x} P^{\text{inc}}[M^- e^{-i\sqrt{n^2 k^2 - k_x^2}\, y} + M^+ e^{i\sqrt{n^2 k^2 - k_x^2}\, y}]
\end{aligned}
\right\}
\tag{2.6}
$$

and
$$
p(x, y \leq 0) = e^{ik_x x} P^{\text{inc}} T\, e^{-i\sqrt{n_s^2 k^2 - k_x^2}\, y}.
$$

This one-dimensional problem can be solved owing to the continuity relations imposed by the structure of equations (1.1) (continuity of $p(x, y)$ and continuity of $a(y)\partial_y p(x, y)$). We have

$$
\left.
\begin{aligned}
p(x, 0^-) &= p(x, 0^+), \quad a_s \partial_y p(x, 0^-) = a \partial_y p(x, 0^+) \\
p(x, \ell^-) &= p(x, \ell^+), \quad a \partial_y p(x, \ell^-) = \partial_y p(x, \ell^+).
\end{aligned}
\right\}
\tag{2.7}
$$

and

Next, (R, T), (M^+, M^-) can be calculated easily, and we report the result for R

$$
R = \frac{\xi(1 - Z) + i(1 - Z\xi^2)\tan k_w \ell}{\xi(1 + Z) - i(1 + Z\xi^2)\tan k_w \ell},
\tag{2.8}
$$

where we have introduced

$$
\left.\begin{aligned}
k_w &\equiv \sqrt{n^2 k^2 - k_x^2}, \\
\xi &\equiv \frac{\sqrt{k^2 - k_x^2}}{a k_w} \quad \text{and} \quad Z \equiv \frac{a_s \sqrt{n_s^2 k^2 - k_x^2}}{\sqrt{k^2 - k_x^2}},
\end{aligned}\right\}
\tag{2.9}
$$

and we chose the convention $\sqrt{-1} = +i$. Here, k_w is simply the wavenumber along y in the slab Ⓑ. ξ and Z are the ratio of the impedances, respectively, between media Ⓐ and Ⓑ and between Ⓐ and Ⓒ. $M^\pm$ and T are not given but it is easy to show that they have the same denominator as R. Let us take

$$
P^{\text{inc}} = \xi(1 + Z) - i(1 + Z\xi^2) \tan k_w \ell,
\tag{2.10}
$$

the common denominator of R, $M^\pm$ and T. It is clear from equation (2.8) that, if $P^{\text{inc}} = 0$ (note that then $P^{\text{inc}} R \neq 0$), then the problem equation (2.6) is no longer a scattering problem, but it is a homogeneous problem, and the solution in equation (2.6) is a guided wave solution of (2.4) with $r = P^{\text{inc}} R$, $m^\pm = P^{\text{inc}} M^\pm$ and $t = P^{\text{inc}} T$. In other words, the scattering problem (2.6) with a non-vanishing amplitude of the incident wave ($P^{\text{inc}} = 1$ for instance) and divergent scattering coefficients $(R, T, M^\pm)$ is equivalent to the homogeneous problem (2.4) with finite coefficients $(r, t, m^\pm)$. It follows that the dispersion relation of guided waves is obtained for $k_x = \beta(k)$ in equations (2.9) and

$$
\xi(1 + Z) = i(1 + Z\xi^2) \tan k_w \ell.
\tag{2.11}
$$

(b) Classical guided waves in a homogeneous anisotropic waveguide

We now extend the previous calculation to the case where the slab is anisotropic with the principal directions of anisotropy (X, Y) being tilted by an angle α with respect to (x, y). The problem is reduced to the same exercise as previously (with $P^{\text{inc}} = 1$), namely solving

$$
\left.\begin{aligned}
p(x, y \geq \ell) &= e^{ik_x x}[e^{-i\sqrt{k^2 - k_x^2} y} + R\, e^{i\sqrt{k^2 - k_x^2} y}], \\
p(x, 0 < y \leq \ell) &= e^{ik_x x}[M^+ e^{i\kappa^+ y} + M^- e^{-i\kappa^- y}]
\end{aligned}\right\}
\tag{2.12}
$$

and

$$
p(x, y \leq 0) = e^{ik_x x} T\, e^{-i\sqrt{n_s^2 k^2 - k_x^2} y},
$$

and the difference is only that the component of the wavevectors along y in the slab $0 < y \leq \ell$, denoted $\kappa^\pm$, are not just of opposite signs. Indeed, in the (x, y) frame, the wave propagation is described by $\nabla \cdot [a \nabla p] + b k^2 p = 0$ with

$$
a = \begin{pmatrix} a_x & a_{xy} \\ a_{xy} & a_y \end{pmatrix},
\tag{2.13}
$$

and

$$
\left.\begin{aligned}
a_x &\equiv a_o \sin^2 \alpha + a_e \cos^2 \alpha, \\
a_y &\equiv a_o \cos^2 \alpha + a_e \sin^2 \alpha \\
a_{xy} &\equiv (a_e - a_o) \cos \alpha \sin \alpha
\end{aligned}\right\}
\tag{2.14}
$$

(see [15]). The wave equation is $[a_x \partial_{x^2} + a_y \partial_{y^2} + 2a_{xy} \partial_x \partial_y + b k^2] p = 0$. Looking for a solution of the plane wave in the form $e^{i(k_x x + \kappa y)}$ leads to the dispersion relation $D(k_x, \kappa; k) = a_x k_x^2 + a_y \kappa^2 + 2a_{xy} k_x \kappa - b k^2 = 0$, leading to

$$
\kappa^\pm = -\frac{a_{xy}}{a_y} k_x \pm \sqrt{\frac{b}{a_y} k^2 - \frac{a_o a_e}{a_y^2} k_x^2}
\tag{2.15}
$$

(and we have used $a_x a_y - a_{xy}^2 = a_o a_e$). Next, to get the scattering coefficients (R, T) in equation (2.12), the continuity relations at the interfaces $y = 0$ and $y = \ell$ are imposed by the

structure of the equation (2.1), namely the continuity of the field p and the continuity of the normal component of the vector $\mathfrak{a}\nabla p$. This leads to

$$p(x, 0^-) = p(x, 0^+), \quad a_s \partial_y p(x, 0^-) = a_y \partial_y p(x, 0^+) + a_{xy} \partial_x p(x, 0^+) \Big\}$$

and

$$p(x, \ell^-) = p(x, \ell^+), \quad a_y \partial_y p(x, \ell^-) + a_{xy} \partial_x p(x, \ell^-) = \partial_y p(x, \ell^+). \Big\} \tag{2.16}$$

We get the same expression of R as in equation (2.8), the same dispersion relation of the guided waves as in equation (2.11), but now

$$
k_w = \frac{n_o/n_e}{\cos^2 \alpha + n_o^2/n_e^2 \sin^2 \alpha} \sqrt{n_e^2(\cos^2 \alpha + n_o^2/n_e^2 \sin^2 \alpha)k^2 - k_x^2},
$$

$$
\xi \equiv \frac{\sqrt{k^2 - k_x^2}}{a_y k_w} \quad \text{and} \quad Z \equiv \frac{a_s\sqrt{n_s^2 k^2 - k_x^2}}{\sqrt{k^2 - k_x^2}}. \tag{2.17}
$$

The expressions of (k_w, ξ, Z) in the isotropic case equation (2.9) are recovered obviously from the expressions in equations (2.17) for $n = n_e = n_o$. Note that for $\alpha = 0$, $k_w = \kappa^+$ ($a_{xy} = 0$, $a_y = a_o$).

(c) General considerations in the (k_x, k) plane

Now we inspect the conditions for which a guided wave can take place in the (k_x, k) plane. Figure 3 shows the reflection coefficient $|R|$ of the slab for the anisotropic problem, equation (2.12) (R is given by equations (2.8) and (k_w, ξ) given by equations (2.17)); the incident wave is described in the (k_x, k) plane. Several regions are drawn in this plane, delimited by the light lines of equation $k_x = Nk$ with N a refractive indice, which separate the region where waves are propagating in the y-direction $k_x < Nk$, from the region where waves are evanescent in the y-direction $k_x > Nk$. In the media Ⓐ and Ⓒ, $N = 1$ and n_s, respectively, and in the layer Ⓑ, $N = \sqrt{n_e^2 \cos \alpha^2 + n_o^2 \sin \alpha^2}$ (see k_w in equation (2.17)). We have considered an anisotropic slab: in the slab Ⓑ, $\alpha = 0$, $b = 1$, $a_o = 0.5$, $a_e = 0.02$ ($N = n_e \simeq 7.1$) and in Ⓒ, $b_s = 1$, $a_s = 0.1$ ($n_s \simeq 3.2$).

It yields the regions ① to ④ in figure 3. In Region ①, above the light line for vacuum $k_x = k$, the waves are propagating in all the media Ⓐ, Ⓑ and Ⓒ. There, perfect transmissions $R = 0$ can take place if the impedance matching condition is satisfied at each interface $y = 0, \ell$ [20,23]. Next, in Region ② above the line $k_x = n_s k$, the wave is evanescent in the vacuum and propagating both in the slab Ⓑ and in the substrate Ⓒ; it follows that only quasi-resonances (with finite amplitude) can occur. In Region ③ above the line $k_x = n_e k$, the incident wave and the transmitted wave are evanescent while the wave in the slab Ⓑ is propagating (since $1 < n_s < n_e$); There, guided modes (called also spoof plasmons) can take place. Eventually, the region ④ below the line $k_x = n_e k$, where the waves are evanescent in all media can give rise to surface plasmon resonances at the interfaces.

Obviously, the existence of these regions does not mean that the phenomena of perfect transmission or of plasmonic resonances will be observed. In the example of figure 3, we observe perfect transmissions in the Region ① (deep blue lines corresponding to $|R| = 0$), quasi resonances (Region ②) and resonances of spoof plasmons (Region ③), with light red lines and bright red lines corresponding, respectively, to large and infinite $|R|$ values in our scattering problem. Next, the chosen configuration does not support surface plasmon (no resonances are observed in Region ④). Resonances in the Region ④ mean that waves are guided at the two interfaces Ⓐ–Ⓑ and Ⓑ–Ⓒ while being evanescent in the three media Ⓐ, Ⓑ and Ⓒ. In other words, each single interface ($\ell = 0$ for a succession of media Ⓐ–Ⓑ or Ⓑ–Ⓒ) has to support surface waves. For $\ell = 0$, the dispersion relation, equation (2.11), is satisfied for $Z = -1$, and consequently, from equation (2.17), $a_s < 0$. These are the classical surface plasmons which occur only for negative permittivity ε (and $a_s = 1/\varepsilon$), as the interface between air and metals in the visible range. More precisely equation (2.17) leads to

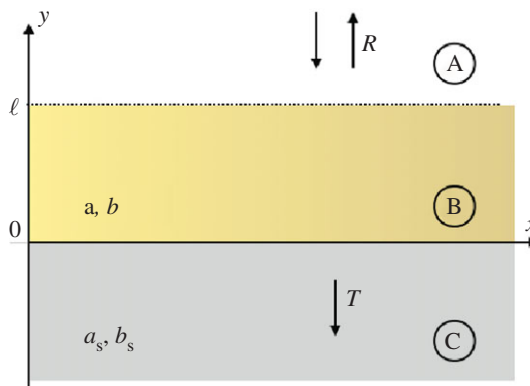$$\beta(k) = k\sqrt{\frac{\varepsilon}{1 + \varepsilon}}.$$

7

rspa.royalsocietypublishing.org Proc. R. Soc. A **471**: 20150472

Figure 2. Scattering problem by an homogeneous anisotropic slab of thickness ℓ. The slab material is characterized by the matrix a and the scalar b. (Online version in colour.)
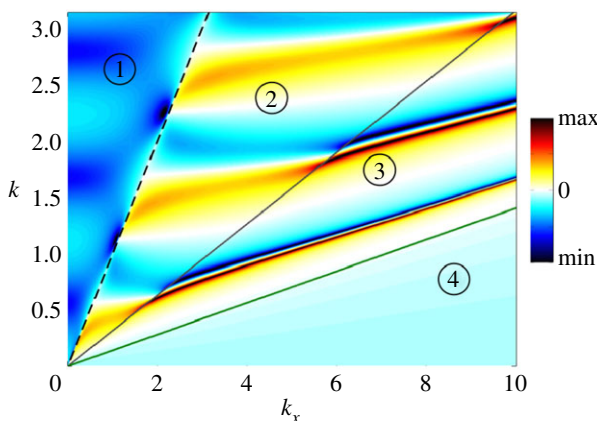

Figure 3. Reflection coefficient $\log |R|$ in the (k_x, k) plane; the incident wave is $e^{i(k_x x + k_y y)}$ with $k_x^2 + k_y^2 = k^2$ for an anisotropic slab (figure 2) of length $\ell = 2$. The parameters of the materials in Ⓑ and Ⓒ are $(a_o, a_e) = (0.5, 0.02)$, $b = 1$ and $a_s = 0.1$, $b_s = 1$. The regions ① to ④ correspond to different behaviours (propagating or evanescent) of the waves in the media Ⓐ, Ⓑ and Ⓒ. (Online version in colour.)

Note that in figure 3, we report $\log |R|$ in colourscale. Because $0 \leq |R| \leq +\infty$, the log representation highlights the perfect transmissions $|R| = 0$ and the resonances $|R| \rightarrow +\infty$. Nevertheless, the colourbar is given in terms of min and max only, since their values depend on the discretization chosen for k_x and k (perfect transmissions can reach arbitrary large negative values of $\log |R|$ and perfect resonances arbitrary large positive values of $\log |R|$).

3. The case of a microstructured slab using homogenization theory of layered media

(a) From plasmonic waves to guided waves

(i) The homogenization theory of layered media

We briefly recall the homogenization theory at zero order for the wave equation $\nabla \cdot (a \nabla p) + b$ $k^2 p = 0$ in a two-dimensional d-periodic medium, with $a(x, y)$ and $b(x, y)$ being periodic functions
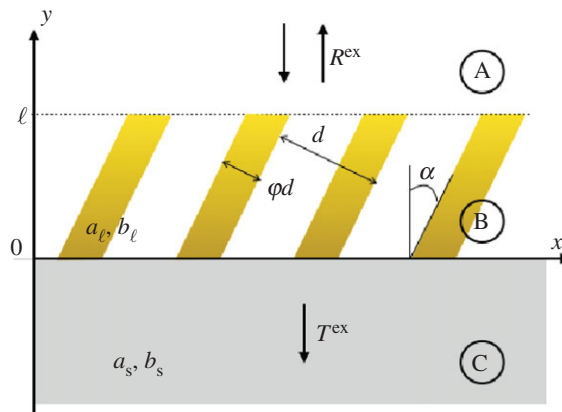
Figure 4. Scattering problem for a structured thick interface between air Ⓐ and a substrate Ⓒ. The microstructure is made of tilted layers alternating a material of parameters (a_ℓ, b_ℓ) and air. (Online version in colour.)

in the unit cell $(x, y) \in [0, d]^2$. At leading order, p can be approximated by p^0 solution of

$$\nabla \cdot (\mathbf{a}^\star \nabla p^0) + k^2 \langle b \rangle p^0 = 0,$$

where $\langle . \rangle$ denotes the spatial average over the unit cell. $\mathbf{a}^\star$ is a 2×2 matrix defined by

$$\mathbf{a}^\star = \left\langle a \begin{pmatrix} 1 + \dfrac{\partial w_1}{\partial x} & \dfrac{\partial w_2}{\partial x} \\ \dfrac{\partial w_1}{\partial y} & 1 + \dfrac{\partial w_2}{\partial y} \end{pmatrix} \right\rangle,$$

where the functions $w_1(x, y)$ and $w_2(x, y)$ are d-periodic along x and y, satisfying the so-called cell problems [16]

$$\frac{\partial}{\partial x} \left[a \left(1 + \frac{\partial w_1}{\partial x} \right) \right] + \frac{\partial}{\partial y} \left(a \frac{\partial w_1}{\partial y} \right) = 0,$$

$$\frac{\partial}{\partial x} \left(a \frac{\partial w_2}{\partial x} \right) + \frac{\partial}{\partial y} \left[a \left(1 + \frac{\partial w_2}{\partial y} \right) \right] = 0.$$

The layered case $a(x, y) = a(x)$ leads to explicit solutions of the cell problems, with $w_i(x, y) = w_i(x)$. We immediately get $a^\star_{21} = 0$ and $a^\star_{22} = \langle a \rangle$. Next, the cell problems reduce to $[a(1 + w'_1)]' = 0$ and $(aw'_2)' = 0$ (where prime denotes the derivative with respect to x). The first relation gives $w'_1(x) = C_1/a(x) - 1$ with C_1 an unknown constant; the periodicity condition leads to $\langle w'_1 \rangle = 0$ which provides the value $C_1 = \langle a^{-1} \rangle^{-1}$; this leads to $a^\star_{11} = \langle a(1 + w'_1) \rangle = C_1$. The second relation gives $w'_2(x) = C_2/a(x)$ and the periodicity condition gives now $C_2 = 0$, from which $a^\star_{12} = \langle aw'_2 \rangle = 0$. To conclude, the effective tensor is simply

$$\mathbf{a}^\star = \begin{pmatrix} \langle a^{-1} \rangle^{-1} & 0 \\ 0 & \langle a \rangle \end{pmatrix}. \tag{3.1}$$

(ii) Application to a microstructured thick interface

We consider the case where the anisotropy of the slab results from a subwavelength microstructure corresponding to layers regularly spaced with spacing d being at subwavelength scale, namely $kd \ll 1$ (figure 4). The structure consists in layers of length φd (φ is a filling fraction) and is made of a material with parameters (a_ℓ, b_ℓ) regularly spaced in the air (note that no further complication arises if we replace the air by another material).

When $\alpha = 0$, the homogenization theory provides for the slab Ⓑ an equivalent effective medium described by $a = a^\star$ of equation (3.1) and by $b = \langle b(x) \rangle$. $a^\star$ can be compared to a of equation (2.2) with $a_e = \langle a^{-1} \rangle^{-1}$, $a_o = \langle a \rangle$. The averages reduce to

$$
\left.
\begin{aligned}
a_o &= \varphi a_\ell + (1 - \varphi), \\[4pt]
a_e &= \left[\frac{\varphi}{a_\ell} + (1 - \varphi) \right]^{-1} \\[4pt]
b &= \varphi b_\ell + (1 - \varphi).
\end{aligned}
\right\}
\tag{3.2}
$$

and

When $\alpha \neq 0$, the slab is described in terms of the a tensor in equations (2.13) and (2.14), with the above values of (a_o, a_e, b). From the definition of n_e and n_o in equation (2.3), we get

$$
\left.
\begin{aligned}
n_e &= \sqrt{[\varphi b_\ell + 1 - \varphi] \left[\frac{\varphi}{a_\ell} + 1 - \varphi \right]} \\[4pt]
n_o &= \sqrt{[\varphi b_\ell + 1 - \varphi][\varphi a_\ell + 1 - \varphi]^{-1}}.
\end{aligned}
\right\}
\tag{3.3}
$$

and

(b) Inspection of the validity of the homogenized problem

The dispersion relation equation (2.11), obtained in §2 for homogeneous slabs, is exact. In the case of a slab containing a micro structure, the homogenization introduces an approximation and it makes sense to inspect its limits of validity. To do that, we make reference to the scattering problem discussed previously (figure 3). The anisotropy of the layer Ⓑ is now ensured by layers with $a_\ell = \frac{1}{100}$, $b_\ell = 1$ and $\varphi = \frac{1}{2}$ and with some thickness d; using equations (3.2), we get $a_o \simeq 0.5$ and $a_e \simeq 0.02$ as previously. The geometry of the slab corresponds to $\alpha = 0$ and $\ell = 2$, and the substrate Ⓒ has $a_s = 0.1$ and $b_s = 1$.

Obviously, in the homogenized version, d does not exist since it is associated to the scale of the microstructure, which has been lost in the homogenization process; this is why we use dimensional quantities, and k_w is thought in term of arbitrary unit. Because the length scale d is lost, we loose two information simultaneously (i) the smaller scale of the structure that the wave is assumed to feel on average only; if kd becomes of order unity, the wave becomes sensitive to that scale and the homogenization fails and (ii) the periodicity of the structure, which defines the first Brillouin zone $k_x < \pi/d$. With $d \to 0$ in the homogenization process, the size of the Brillouin zone is infinite, and this is not the case for practical cases.

Thus, we inspect the validity of our expression with respect to actual layers with finite d-period. We performed full wave computations [24] for the same range of k values and with $d = 0.1$, 0.2 and 0.3. The results are shown in figure 5. Expectedly, we observe (i) that the homogenization prediction is valid only in the first Brillouin zone, so that a smaller d enlarges the validity of the homogenization prediction in terms of k_x-value by just shifting the limit of the Brillouin zone, (ii) for large kd values ($kd > 0.3 - 0.4$ in figure 5), the homogenization becomes less accurate because smaller wavelengths become sensitive to the actual microstructure.

In the following, these effects are disregarded and we assume that d is small enough so that the captured phenomena are associated to k_x being in the first Brillouin zone and $kd \ll 1$.

(c) The case of perfectly conducting layers, the Neumann limit

A Neumann boundary condition corresponds to vanishing normal derivative of the field at the interfaces. This corresponds to a large impedance of the material, namely $|Z_\ell| = |1/\sqrt{a_\ell b_\ell}| \to \infty$. In electromagnetism, this is the case for perfectly conducting layers in TM polarization (metals in the far infrared regime), where the propagation is described by the wave equation (1.3) with large $|\varepsilon|$-values (negative $\varepsilon = 1/a_\ell$) and $\mu = 1$ ($\mu = b_\ell$). The limit $|\epsilon| \to \infty$ is known to be in conflict with the limit of homogenization, where all the length scales of the microstructure have to be
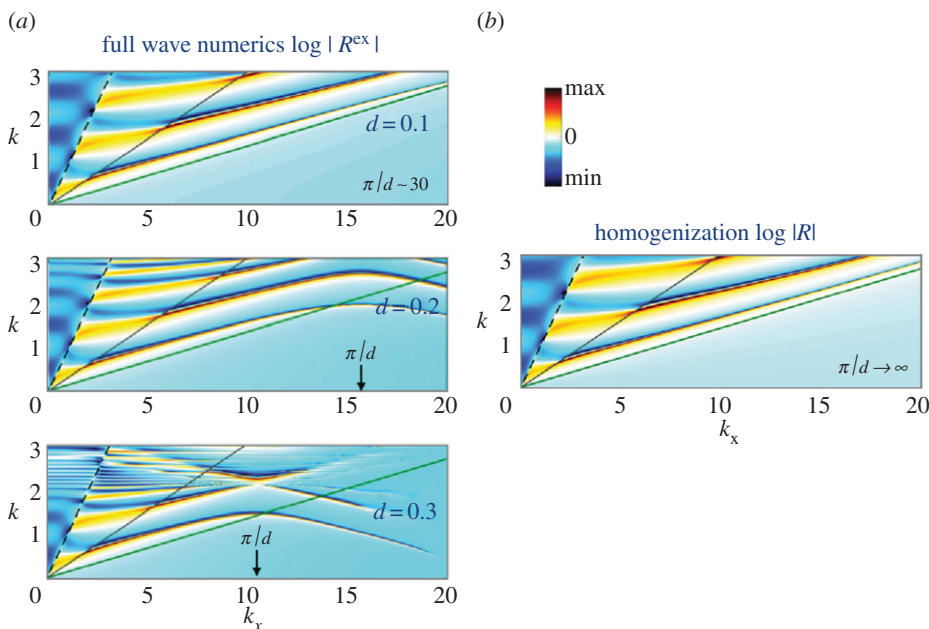
10

rspa.royalsocietypublishing.org   Proc. R. Soc. A **471**: 20150472

(a)

full wave numerics log $|R^{ex}|$

(b)

Figure 5. Reflection coefficients log $|R|$ in the (k_x, k) plane: (a) $|R^{ex}|$ in the actual problem (structured thick interface, figure 4) and (b) $|R|$ in the homogenized problem (figure 3). On (a), the calculations have been performed for the layers spacing $d = 0.1$, 0.2 and 0.3, from top to bottom. (Online version in colour.)
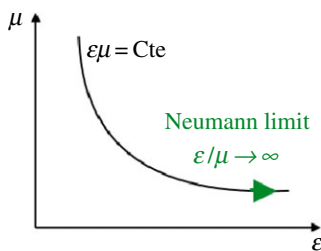

Figure 6. Neumann limit in the (ε, μ) plane remaining valid within homogenization theory. (Online version in colour.)

small compared to all the length scales associated to the wave. The limit $|Z_\ell| = |\sqrt{\varepsilon/\mu}| \to \infty$ is accompanied by a diverging imaginary index $n = \sqrt{\varepsilon\mu}$, and thus a vanishing skin depth; this latter length scale is associated to the wave which explains the conflict. This has been extensively studied and discussed [25–27] to avoid the failure of the homogenization.

This conflict does not appear for acoustic waves. In this context, Neumann boundary conditions are associated to sound hard materials, which have large relative density ρ ($a = 1/\rho$) and large relative bulk modulus $B = \rho c^2$ with c the sound speed ($b = 1/B$). The wave equation for the pressure field p is equation (1.2). Because c does not change much from one material to another, $Z_a = \rho c$ is associated to a large density but the refraction index $n = \sqrt{\rho/B}$ does not increase dramatically (and one may choose to consider constant n value). This means that the wavelength inside such media can be still considered large compared to the microstructure scale and the Neumann limit can be taken within the homogenization limit safely by considering $Z \to \infty$ while considering constant n value. This is similar to the trajectory suggested in [26] for non-magnetic materials, and the trajectory is chosen in the (k, ε) space in this reference (the Neumann limit corresponding to $\varepsilon \to \infty$ and $k \to 0$). By analogy with the acoustic case, our trajectory in the phase space ($b = \mu, a = 1/\epsilon$) is illustrated in figure 6.

This analogy has already been used to easily homogenize layers made of perfectly conducting metals [28] and this is what we will use in the following. With $a_\ell, b_\ell \to 0$ and $a_\ell/b_\ell =$ Cte, equation (3.2) simplifies in $a_\mathrm{o} = 1 - \varphi = b, a_\mathrm{e} = 0$, and equation (2.14) gives $a_y = (1 - \varphi)\cos^2\alpha$ (note that to take $b_\ell = \mu = 1$ as in the real medium would lead to the wrong result $b = 1$ instead of $1 - \varphi$). Then ξ and k_w in equation (2.17) are deeply simplified, with $n_\mathrm{o} = 1$, $n_\mathrm{e} = \infty$, in

$$k_\mathrm{w} = \frac{k}{\cos\alpha} \quad \text{and} \quad \xi = \frac{\sqrt{k^2 - k_x^2}}{k(1 - \varphi)\cos\alpha}, \tag{3.4}$$

and as expected, the result does not depend on the value of the constant a_ℓ/b_ℓ.

4. Examples

In this section, we give examples of guided waves in particular geometries. First, we recover the classical spoof plasmon for a grating [17–19] in the context of electromagnetic waves, which corresponds to metallic layers supported by a metallic substrate (medium ©) (in a frequency range where metal can be associated to Neumann boundary conditions); we also consider the case of an array where the metallic layers form an array surrounded by air (the medium © is identical to Ⓐ). Next, we consider guided waves by an array in the context of acoustic waves and we inspect the influence of the layer material, from the limit of sound hard material to sound soft material.

(a) Electromagnetic waves: dispersion relation of spoof plasmons

As previously discussed, the Neumann limit is taken considering vanishing a and b values and a finite b/a value. This is the right boundary condition to be applied on the interface with a perfectly conducting metal for transverse magnetic polarization of the wave (the magnetic field $\mathbf{H} = H(x, y)\mathbf{e_z}$ is perpendicular to the incidence plane and $E_z = 0$). We recall that this boundary condition reflects the continuity relation of the component of the electric field $\mathbf{E}(\mathbf{x}, \mathbf{y})$ tangent to the interface, $\mathbf{E} \times \mathbf{n} = \mathbf{0}$ (with $\mathbf{n}$ the unit vector normal to the interface, and because the electric field is zero inside a perfect conductor). Next, with $\nabla \times \mathbf{H} \propto \mathbf{E}$, we get $\mathbf{E} \times \mathbf{n} = \nabla H . \mathbf{n} = 0$. Note that since the magnetic field is also zero inside a perfect conductor, the continuity of the component of $\mathbf{H}$ perpendicular to the interface leads to $\mathbf{H}.\mathbf{n} = 0$ which is automatically satisfied for transverse magnetic polarization.

(i) The case of gratings

For a grating, both the layers and the substrate © are perfectly conducting metal, which corresponds to $a_\mathrm{s} = a_\mathrm{l} \to 0$, $b_\mathrm{s} = b_\mathrm{l} \to 0$ with $n_\mathrm{s} =$ cst. Thus, from equation (2.17), we have $Z = 0$, and the condition of resonance, equation (2.11), simplifies to

$$\xi = \mathrm{i}\tan k_w \ell, \tag{4.1}$$

with (k_w, ξ) given by equation (3.4). We note $k_x = \beta(k)$ the solution, which exists only if $\beta > k$ and if $\tan(k_\mathrm{w}\ell) > 0$: indeed, then we have

$$\xi = \mathrm{i}\frac{\sqrt{\beta^2 - k^2}}{k(1 - \varphi)\cos\alpha}, \tag{4.2}$$

with our convention for the square roots. We get the explicit dispersion relation

$$\beta = k\left[1 + (1 - \varphi)^2\cos^2\alpha\tan^2\left(\frac{k\ell}{\cos\alpha}\right)\right]^{1/2}, \quad \tan\left(\frac{k\ell}{\cos\alpha}\right) > 0, \tag{4.3}$$

and this dispersion relation is usually given for $\alpha = 0$ [17–19]. Note that the restriction to $\tan(k\ell/\cos\alpha) > 0$ is not indicated in these references, where the authors are interested in the first
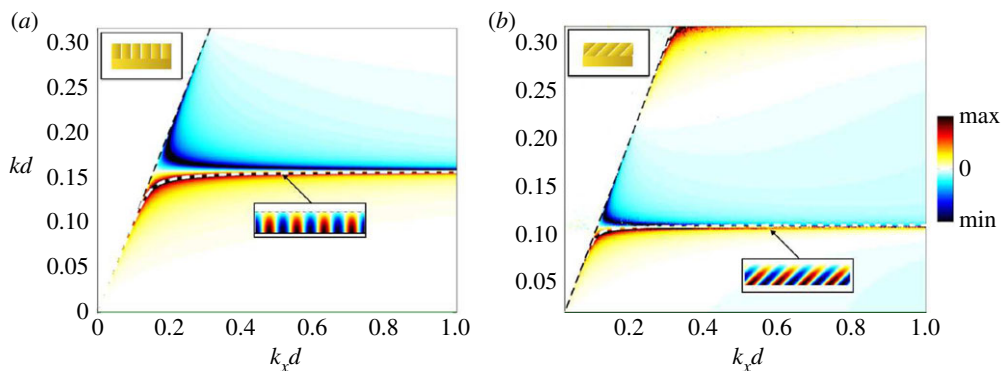
Figure 7. Dispersion relation of the spoof plasmon in a perfect metal grating, $\log |R^{ex}|$ (calculated in the actual structure, with $\ell/d = 10$, $\varphi = 0.9$) is represented in colourscale, and the dispersion relation is visible by means of $\log |R^{ex}| \rightarrow \infty$ reaching large values. Two orientations of the layers are considered: (a) $\alpha = 0$ and (b) $\alpha = \pi/4$. In (a,b), the dashed white lines show the dispersion relations equation (4.3), and the dashed black line is the air light line $k = k_x$. The insets on the top left show the geometry of the structure and the insets with arrows show the wavefields calculated numerically at a resonance for (k_x, k)-values satisfying the dispersion relation (equation (4.3)). (Online version in colour.)

branch only. Inspecting the expression of the reflection coefficient R in equation (2.8), a negative value of $\tan(k\ell/\cos\alpha)$ can produce a vanishing R value, for $\xi = -i\tan k_w\ell$. The band gap in between is visible.

Figure 7 shows the logarithm of the reflection coefficient $\log |R^{ex}|$ in the (k_x, k) plane, calculated numerically for an actual metallic grating (with $d = 0.1$ and $\ell = 1$). The parameters of the grating are $\varphi = 0.9$, and we have considered $\alpha = 0$ and $\pi/4$. In our scattering problem, resonance of evanescent waves (below the light line $k = k_x$ in dashed black line) are visible by means of diverging $\log |R^{ex}|$ values (red areas). We reported for comparison the dispersion relation, equation (4.3) (dashed white curves). For both values of α, the agreement is good; note that increasing α produce a decrease in the asymptotic of the first branch ($k\ell \simeq (\pi/2)\cos\alpha$), revealing the second branch starting at $k\ell = \pi\cos\alpha$ according to the condition $\tan(k\ell/\cos\alpha) > 0$. Curves of perfect transmission $|R^{ex}| = 0$ ($\log |R^{ex}| = -\infty$, blue areas) are located in the areas where $\tan(k\ell/\cos\alpha) < 0$ (here, $\pi/2 < k\ell/\cos\alpha < \pi$).

(ii) The case of arrays

The case of arrays ($\mathbb{C} = \mathbb{A}$, thus $a_s = 1$, $b_s = 1$) has a significant simplification, with $Z = 1$ in equation (2.11), leading to the dispersion relation with two branches

$$
\left.
\begin{aligned}
\xi &= i\tan\left(\frac{k_w\ell}{2}\right) \\
\text{and} \quad \xi &= \frac{1}{i\tan(k_w\ell/2)}.
\end{aligned}
\right\}
\tag{4.4}
$$

With ξ given by equation (4.2), it leads to the dispersion relations

$$
\left.
\begin{aligned}
\beta &= k\left[1 + (1-\varphi)^2\cos^2\alpha\tan^2\frac{k\ell}{2\cos\alpha}\right]^{1/2}, \quad \text{for } \tan\frac{k\ell}{2\cos\alpha} > 0, \\
\text{and} \quad \beta &= k\left[1 + (1-\varphi)^2\cos^2\alpha\cot an^2\frac{k\ell}{2\cos\alpha}\right]^{1/2}, \quad \text{for } \tan\frac{k\ell}{2\cos\alpha} < 0.
\end{aligned}
\right\}
\tag{4.5}
$$

The branches corresponding to $\tan(k_w\ell/2) > 0$ are the same branches as for the grating, with $\ell \rightarrow \ell/2$; they correspond to similar wave patterns: for $\alpha = 0$, on figure 8a, the field associated with
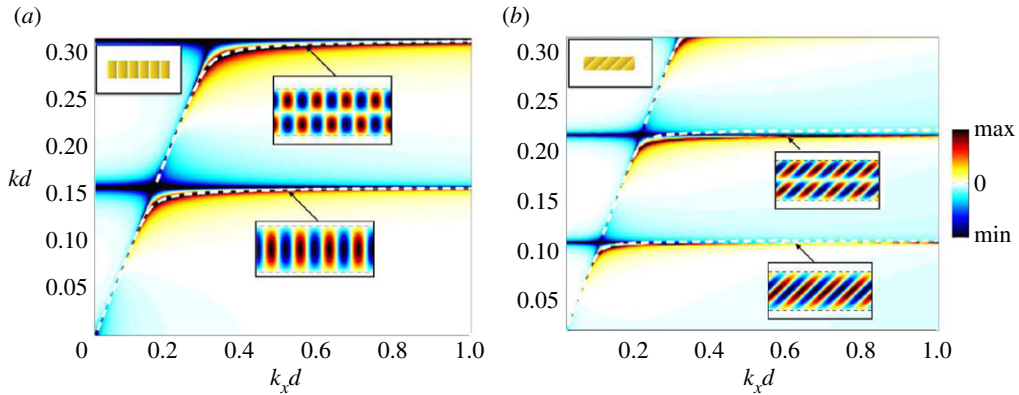
Figure 8. Dispersion relation of the spoof plasmon in an array of perfectly conducting inclusions (same representation as in figure 7). The actual structure has dimensions $\ell/d = 20$ and $\varphi = 0.9$ and different orientations: (a) $\alpha = 0$ and (b) $\alpha = \pi/4$. The dashed white lines show the dispersion relations equation (4.5). (Online version in colour.)
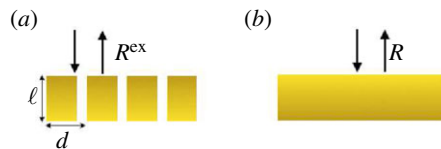

Figure 9. Configuration of (a) the actual microstructured thick interface made of a penetrable material and (b) the equivalent homogenized slab. (Online version in colour.)

the first branch is symmetric with respect to $y = \ell/2$ and is the same (up to a factor 2 dilatation) for $\ell/2 \le y \le \ell$ that the field on figure 7a for $0 \le y \le \ell$. The branches corresponding to $\tan(k_w \ell/2) < 0$ were forbidden in the array; they correspond to antisymmetric wave fields (vanishing at $y = \ell/2$). It follows that the metallic array does not present band gaps.

We show in figure 8 the same quantities as in figure 7; we choose an array with $\ell = 2$ to recover the same asymptotes as for the grating. Again, the agreement is good between the dispersion relations in the homogenized problem (white curves) and in the actual structure (red areas).

(b) Acoustic waves: from sound hard to sound soft array of inclusions

In this section, we focus on the influence of the material properties of the inclusions forming an array in a surrounding medium (figure 9a). Thus, the effect of tilting the inclusions is disregarded and we consider in the following $\alpha = 0$. The basic idea behind this study is to inspect whether or not guided waves exist for different material properties of the inclusions and how the material properties influence the characteristics of these waves, when they exist. To do that, we focus on the case of acoustic waves, with the material properties being the mass density $\rho = 1/a$ and the bulk modulus $B = 1/b$, equation (1.2), and we introduce also the sound speed c which is more common for acoustics ($B = \rho c^2$). The trajectory in the (ρ, c) space to go from sound hard to sound soft material is first chosen, and the limits along this trajectory are inspected. Next, the characteristics of the first guided wave (first branch of the dispersion relation) is regarded, revealing the increase in the ratio β/k for softer material. This is relevant when one thinks of applications to subwavelength imaging or subwavelength guiding. Finally, we discuss the link with inclusions associated to Neumann and Dirichlet boundary condition.
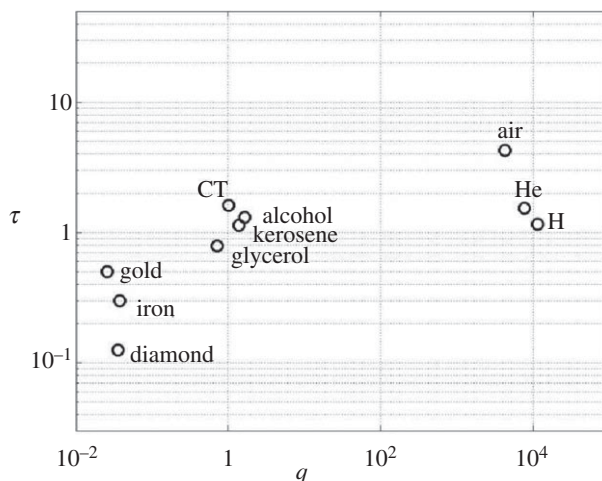
Figure 10. Typical values of the impedance ratio q and of the celerity ratio τ for a surrounding medium being water. For increasing q, we have the solid inclusions (and $\tau < 1$), liquid inclusions (and $\tau \sim 1$) and inclusions of gas ($\tau > 1$). The variations of q are much significative than the variations of τ. (CT stands for carbon tetrachloride and He, H stand for helium and hydrogen.)

(i) Choice of one trajectory from sound hard to sound soft materials

The notion of sound hard/soft material is linked to the ratio of impedances between the surrounding medium ($\mathbb{A} = \mathbb{C}$) and the inclusions. In the context of acoustic waves, the impedance is defined as $\rho c = \sqrt{\rho B}$ (as already discussed in §3c) and we define the ratio of impedances q in equation (4.6), with ρ_ℓ and c_ℓ being the relative mass density and the relative sound speed with respect to the surrounding medium. We also introduce τ being the inverse of the relative sound speed of the inclusions. Our two parameters are

$$
\left.
\begin{aligned}
\tau &\equiv \frac{1}{c_\ell} \\
q &\equiv \frac{1}{\rho_\ell c_\ell}.
\end{aligned}
\right\}
\tag{4.6}
$$

and

This choice is not casual. Usual material have a rather constant velocity for sound waves (about one order of magnitude, 1–10 km s^{-1}) and it is mainly the mass density which varies (with three orders of magnitude, for instance air and water). It is thus quite natural to consider that τ is constant and q varies from 0 (sound hard material) to ∞ (sound soft material), and it is the trajectory we consider in the following. In the case where the surrounding medium is water, we report in figure 10 typical (q, τ) values for inclusions being solids, liquids and gas. While τ is not constant, its amplitude of variation is clearly much smaller than the amplitude of variation of q.

(ii) Behaviour of the guided waves for varying q

We start by expressing the terms of our tensor a in the homogenized problem in terms of (τ, q): (a_ℓ, b_ℓ) with $a_\ell = 1/\rho_\ell = q/\tau$ and $b_\ell = 1/B_\ell = q\tau$. From (2.14) and (3.2), we get

$$
\left.
\begin{aligned}
a_x = a_e &= \left(\varphi \frac{\tau}{q} + 1 - \varphi \right)^{-1}, \\
a_y = a_o &= \varphi \frac{q}{\tau} + 1 - \varphi \\
b &= \varphi \tau q + 1 - \varphi,
\end{aligned}
\right\}
\tag{4.7}
$$

and

and $a_{xy} = 0$ for $\alpha = 0$. The dispersion relation remains the same as in equation (4.4),

$$
\left.
\begin{aligned}
\xi &= i \tan\left(\frac{k_w \ell}{2}\right), && \text{for } \tan\left(\frac{k_w \ell}{2}\right) > 0, \\
\text{and} \qquad \xi &= \frac{1}{i \tan(k_w \ell/2)}, && \text{for } \tan\left(\frac{k_w \ell}{2}\right) < 0,
\end{aligned}
\right\}
\tag{4.8}
$$

with ξ and k_w being expressed in terms of (τ, q) (see equations (2.17) and (3.3))

$$
\left.
\begin{aligned}
\xi &= f(\tau, q) \sqrt{\frac{k^2 - k_x^2}{n_e^2 k^2 - k_x^2}} \\
k_w &= g(\tau, q) \sqrt{n_e^2 k^2 - k_x^2},
\end{aligned}
\right\}
\tag{4.9}
$$

and

$$
\left.
\begin{aligned}
n_e &\equiv \left[(\varphi \tau q + 1 - \varphi)\left(\frac{\varphi \tau}{q} + 1 - \varphi\right) \right]^{1/2}, \\
f(\tau, q) &\equiv \left(\frac{\varphi q}{\tau} + 1 - \varphi\right)^{-1/2} \left(\frac{\varphi \tau}{q} + 1 - \varphi\right)^{1/2} \\
g(\tau, q) &\equiv \left[\left(\frac{\varphi q}{\tau} + 1 - \varphi\right)\left(\frac{\varphi \tau}{q} + 1 - \varphi\right) \right]^{-1/2}.
\end{aligned}
\right\}
\tag{4.10}
$$

We focus now on a particular geometry (figure 9a) with $\ell = 3d$, $\varphi = 0.7$ and $\tau = 1.25$ ($\tau > 1$ ensures that a guided wave exists for any value of q and φ, see appendix A) and we consider varying q. In the actual array, R^{ex} refers to the reflection coefficient of this structure, that we compute numerically. In the homogenized problem (figure 9b), R is calculated, equation (2.8) with equations (4.9) and (4.10). The reflection coefficient $|R^{ex}|$ as a function of k and k_x is reported in figure 11a and compared with the reflection coefficient R in the homogenized problem (figure 11b), for $q = 10^{-6}$, 10^{-1}, 10 and 10^2. The agreement is excellent in all cases.

In figures 11, the dispersion relation of the guided waves is visible by means of diverging $|R^{ex}|$ and $|R|$, respectively (red zones). As already said, the guided waves take place in the regions of the (k_x, k)-space below the sound line of the air ($k < k_x$) and above the sound line of the birefringent layer in the homogenized problem ($n_e k > k_x$, dashed white lines, with $n_e > 1$ since $\tau > 1$). The index n_e is close to infinity for $q \to 0$ and the corresponding sound line corresponds to $k = 0$ (the wave is then always propagating in the slab with wavenumber k along y). Increasing q towards unity first produces a decrease of n_e and thus, an increase of the slope of the sound line $n_e k = k_x$ (with maximum value being ($\varphi \tau + 1 - \varphi$) reached for $q = 1$, leading to a transparent effective medium if $\tau = 1$). During this first phase, the wavenumber of the first (lowest frequency) guided wave $k_x = \beta(k)$ (in red) appears to be almost unaffected, with roughly $\beta/k \leq \ell/d$ ($\beta \leq \pi/d$ in the first Brillouin zone). Increasing further $q > 1$ produces an increase in n_e (and a decrease in the slope of the sound line of the slab). But here, the dispersion relation $\beta(k)$ remains stuck to the sound line with $\beta(k) \simeq n_e k$, resulting in an increase of $\beta/k \simeq n_e$.

This scenario is further illustrated in figure 12, which shows the behaviour of $|R^{ex}|$ as a function of k and q, for a fixed $k_x d = 1$. The dashed white line shows the dispersion relation for the guided wave in the homogenized problem (equation (4.8)). As previously observed, the agreement is excellent between the exact calculation and the analytical dispersion relation of the guided waves in the homogenized problem. The transition is visible between $q < 1$ where the wavenumber of the guided wave remains almost constant, and $q > 1$ where it follows the sound line of the birefringent slab ($k_x = n_e k$). By inspection of equation (4.10), it is easy to see that $q \to \infty$ leads to

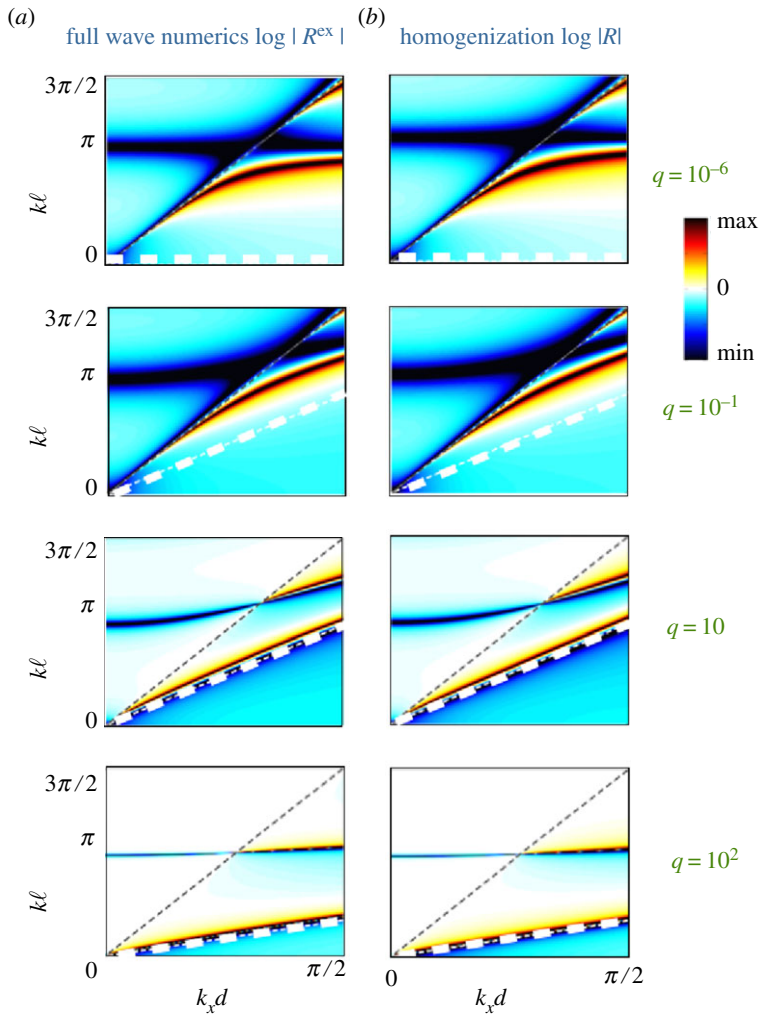**Figure 11.** Reflection coefficient log $|R|$ in the (k_x, k) space for different impedance ratios q (colour scale is in log scale). The (a) panels show log $|R^{ex}|$ calculated numerically and the (b) panels show log $|R|$, equation (2.8) with equations (2.9), in the homogenized calculation. The black dashed line represents the sound line of the air, $k = k_x$. The white dashed line corresponds to the sound line of the birefringent waveguide, $n_e k = k_x$. (Online version in colour.)

$n_e \rightarrow \sqrt{\varphi(1 - \varphi)\tau} \sqrt{q}$ and this scaling law is indeed observed. Finally, it is important to note that the layer sound line has no physical meaning in the real problem.

(iii) Limiting cases $q \rightarrow 0$ and $q \rightarrow \infty$

When considering the simple cases of the scattering by a single circular inclusion or by a plane interface, q is the only parameter which appears and $q \rightarrow 0$ coincides with Neumann boundary condition, while $q \rightarrow \infty$ coincides with Dirichlet boundary condition. Obviously, this cannot be generalized to more involved geometry, as our present array, and this latter has, *a priori*, two degrees of freedom (q, τ).

In the limiting case of sound-hard inclusions, $q \rightarrow 0$, we have, from equations (4.10), $n_e = \sqrt{\varphi(1 - \varphi)\tau}/\sqrt{q} = (1 - \varphi)f = 1/g$. Thus, $n_e g = 1$ and $g \rightarrow 0$, leading to $k_w = k$, and $n_e/f = (1 - \varphi)$ leading to $\xi = i\sqrt{\beta^2 - k^2}/[k(1 - \varphi)]$. We recover the dispersion relation of the equation (4.5), consistent with the dispersion relation derived for inclusions associated to Neumann boundary condition in [17–19].
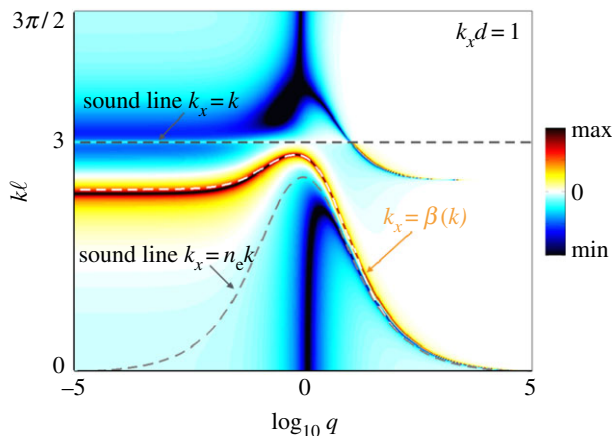
Figure 12. $|R^{ex}|$ in log-scale as a function of k and of the impedance ratio q for $k_x d = 1$ in the actual array (figure 9a). The dispersion relation is visible by means of $|R^{ex}| \to \infty$. White dotted line shows the dispersion relation of the guided wave in the homogenized problem (equation (4.8)) and dotted black lines show the sound lines $k_x = k$ and $k_x = n_e k$. (Online version in colour.)

In the limiting case of sound-soft inclusions, $q \to \infty$, it is shown in appendix B that the dispersion relation of the first guided wave takes the form

$$\beta \simeq \left[\sqrt{\varphi(1-\varphi)\tau q} - \frac{1-\varphi}{k\ell} \right] k. \tag{4.11}$$

As previously said, at dominant order, $\beta \simeq n_e k$, with $n_e = \sqrt{\varphi(1-\varphi)\tau q}$, is close to the light line of the birefringent waveguide. As $q \to \infty$, the ratio of the wavenumbers β/k can reach very high values. This is visible in figure 11: for $q = 10$ and 10^2, the resonances of $|R^{ex}|$ (by means of red regions in the (k_x, k) plane) occur along lines being closer and closer to the horizontal line $k = 0$. Incidentally, the equation 4.11 also indicates that $\beta < n_e k$, which means that the guided wave is propagating along the array of inclusions. It is worth noting that the ratio β/k has a singular limit when $\varphi \to 1$, and $\varphi = 1$ corresponds to an homogeneous slab (instead of the array of disconnected inclusions). Indeed, using $\varphi = 1$ in equations (4.10) gives $n_e = \tau, f = \tau/q$ and $g = 1$, from which the dispersion relation reduces to $\beta \to \tau k$ for $q \to \infty$, and τ is not large. Therefore, a structured array of inclusions can support guided waves with a wavelength much smaller than in a simple layer of the same material; a practical application of this phenomenon has been proposed in [29].

5. Conclusion

We have shown that the classical homogenization theory is able to recover the main features of the guided waves as observed in structured interfaces and structured arrays. This has been done in the simple case of layered media for which analytical expressions of the effective parameters of the equivalent anisotropic medium is available. This allows for the derivation of explicit dispersion relations of the guided waves being, in the homogenized problem, the equivalent of the waves propagating along the actual array or grating. Notably, the dispersion relation of the homogenized problem recover the dispersion relations of plasmons and spoof plasmons for structurations associated with the Neumann boundary condition, and a generalization for tilted layers has been proposed. Beyond the case of structures made of hard materials, the dispersion relation of the homogenized problem has been shown to predict correctly the existence of guided waves by structures made of penetrable materials. Notably, the case of soft materials has been shown to be promising for flexible tuning of the guided wave properties. Improvements in the design of tuneable metamaterials require precise theoretical predictions; with regard to that aim, we think that the homogenization theories are natural and powerful approaches.

Appendix A. Constraint on the τ-value

As previously said in paragraph (c), the dispersion relation equation (2.11) has guided waves solutions if $k < k_x < n_e k$, that is, trapped waves being evanescent in the air and propagating in the slab. This implies $n_e > 1$, which translates, by inspection of equation (4.10), in

$$(\varphi\tau)^2 + (1 - \varphi)^2 + \varphi(1 - \varphi)\tau\left(q + \frac{1}{q}\right) > 1. \tag{A 1}$$

This is obviously satisfied for $\tau = 1$ since $q + 1/q \geq 2$. Otherwise, it is sufficient to remark that $(q + 1/q)$ is minimum at $q = 1$. Thus, the inequality is always satisfied if it is satisfied for $q = 1$, namely $(\varphi\tau)^2 + (1 - \varphi)^2 + 2\varphi(1 - \varphi)\tau = (\varphi\tau + 1 - \varphi)^2 > 1$. Since for $0 < \varphi < 1$, $\varphi\tau + 1 - \varphi$ varies between τ and 1, we get the final condition that $\tau > 1$ or equivalently $c_\ell < 1$, according to equation (4.6): the material must be slower than the outside medium.

Appendix B. Higher branches of the penetrable array

Here, we present the dispersion relations of all the guided waves in the Neumann case. In the limit $q \to \infty$ of sound-soft inclusions, from equations (4.9) and (4.10), we get the simplifications

$$\left.\begin{aligned}
\xi &\sim i\sqrt{\frac{\tau}{q}\frac{1 - \varphi}{\varphi}}\sqrt{\frac{\lambda^2 - 1}{\varphi(1 - \varphi)\tau q - \lambda^2}} \\
\text{and} \qquad k_w &\sim k\sqrt{\frac{\tau}{\varphi(1 - \varphi)q}}\sqrt{\varphi(1 - \varphi)\tau q - \lambda^2},
\end{aligned}\right\} \tag{A 2}$$

where we have noted $\lambda = k_x/k$, satisfying $1 < \lambda < n_e \sim \sqrt{\varphi(1 - \varphi)\tau q}$ to get a guided wave.

Let us concentrate on the first dispersion relation branch $\xi = i\tan(k_w\ell/2)$ for $\tan(k_w\ell/2) > 0$, corresponding to symmetric guided waves. Since $\xi \to 0$ when $q \to \infty$, the solutions of $\xi = i\tan(k_w\ell/2)$ are obtained for $k_w\ell/2 = n\pi + u_n$, $n = 0, 1, 2, \ldots$ and $0 < u_n \ll n\pi$. From equation (A 2), we get

$$\sqrt{\frac{\tau}{q}\frac{1 - \varphi}{\varphi}}\sqrt{\frac{\lambda^2 - 1}{\varphi(1 - \varphi)\tau q - \lambda^2}} \sim k_w\ell/2 - n\pi \sim \frac{kl}{2}\sqrt{\frac{\tau}{\varphi(1 - \varphi)q}}\sqrt{\varphi(1 - \varphi)\tau q - \lambda^2} - n\pi,$$

or equivalently

$$(1 - \varphi)\sqrt{\lambda^2 - 1} \sim \frac{kl}{2}[\varphi(1 - \varphi)\tau q - \lambda^2] - n\pi\sqrt{\frac{\varphi(1 - \varphi)q}{\tau}}\sqrt{\varphi(1 - \varphi)\tau q - \lambda^2}. \tag{A 3}$$

The conclusion depends on the value of n : for $n \neq 0$, since the left-hand side of equation (A 3) does not depend on q, we get for large q the dispersion relation $k_x = \beta(k)$ with

$$k^2 = \left(\frac{2n\pi}{\tau\ell}\right)^2 + \left(\frac{\beta}{n_e}\right)^2, \quad \text{for } \beta > k,$$

where $n_e^2 = \varphi(1-\varphi)\tau q$. For $n = 0$, the previous relation gives $\beta \simeq n_e k$ which is the light line, or sound line, of the birefringent waveguide. To check that $\beta < n_e k$ in order to prove the existence of a guided wave, we have to perform a more precise calculation: starting from equation (A 3) with $n = 0$, we look for a solution of the form $\lambda = n_e - v$ with $0 < v \ll n_e$. Using $\lambda^2 \sim n_e^2 - 2n_e v$ and $n_e \gg 1$, we get v and we deduce the dispersion relation

$$\beta \simeq \left[\sqrt{\varphi(1-\varphi)\tau q} - \frac{1-\varphi}{k\ell} \right] k. \tag{A 4}$$

For the antisymmetric dispersion relation branch $\xi = 1/i \tan(k_w \ell/2)$ for $\tan(k_w \ell/2) < 0$, the solutions are obtained for $k_w \ell/2 = (n - \frac{1}{2})\pi + u_n, n = 1, 2, \ldots$. We get

$$k^2 = \left(\frac{(2n-1)\pi}{\tau\ell} \right)^2 + \left(\frac{\beta}{n_e} \right)^2, \quad \text{for } \beta > k.$$

On figure 11 and $q = 10^2$ ($n_e \sim 5$) are seen the branch $n = 0$ and the branch $n = 1$ of equation

$$(k\ell)^2 = \left(\frac{\pi}{\tau} \right)^2 + \left(\frac{\beta d}{n_e} \frac{\ell}{d} \right)^2, \quad \text{for } \beta > k.$$

The condition $\beta > k$ leads to $\beta d > (\pi n_e/\tau)(1/\sqrt{n_e^2 - 1})(d/\ell) = 0.85$, and this is confirmed on figure 11: the second branch starts at the point $k_x d = 0.85$ and $k\ell = 0.85(d/\ell) = 2.56$.

References

1. Chow E, Lin SY, Wendt JR, Johnson SG, Joannopoulos JD. 2001 Quantitative analysis of bending efficiency in photonic-crystal waveguide bends at $\lambda = 1.55\,\mu$m wavelengths. *Opt. Lett.* **26**, 286–288. (doi:10.1364/OL.26.000286)
2. Mekis A, Chen JC, Kurland I, Fan S, Villeneuve PR, Joannopoulos JD. 1996 High transmission through sharp bends in photonic crystal waveguides. *Phys. Rev. Lett.* **77**, 3787–3790. (doi:10.1103/PhysRevLett.77.3787)
3. Notomi M, Yamada K, Shinya A, Takahashi J, Takahashi C, Yokohama I. 2001 Extremely large group-velocity dispersion of line-defect waveguides in photonic crystal slabs. *Phys. Rev. Lett.* **87**, 253902. (doi:10.1103/PhysRevLett.87.253902)
4. Temelkuran B, Bayindir M, Ozbay E, Biswas R, Sigalas MM, Tuttle G, Ho KM. 2000 Photonic crystal-based resonant antenna with a very high directivity. *J. Appl. Phys.* **87**, 1. (doi:10.1063/1.371817)
5. Mogilevtsev D, Birks TA, Russell PSJ. 1998 Group-velocity dispersion in photonic crystal fibers. *Opt. Lett.* **23**, 1662–1664. (doi:10.1364/OL.23.001662)
6. Enoch S, Tayeb G, Sabouroux P, Guérin N, Vincent P. 2002 A metamaterial for directive emission. *Phys. Rev. Lett.* **89**, 213902. (doi:10.1103/PhysRevLett.89.213902)
7. Choi CJ, Cunningham BT. 2006 Single-step fabrication and characterization of photonic crystal biosensors with polymer microfluidic channels. *Lab Chip* **6**, 1373–1380. (doi:10.1039/b603514k)
8. Asatryan AA, Botten LC, Byrne MA, Freilikher VD, Gredeskul SA, Shadrivov IV, McPhedran RC, Kivshar YS. 2007 Suppression of anderson localization in disordered metamaterials. *Phys. Rev. Lett.* **99**, 193902. (doi:10.1103/PhysRevLett.99.193902)
9. Maurel A, Ourir A, Mercier JF, Pagneux V. 2012 Usual anderson localization restored in bilayered left- and right-handed structures. *Phys. Rev. B* **85**, 205138. (doi:10.1103/PhysRevB.85.205138)
10. Kadic M, Bückmann T, Schittny R, Gumbsch P, Wegener M. 2014 Pentamode metamaterials with independently tailored bulk modulus and mass density. *Phys. Rev. Appl.* **2**, 054007. (doi:10.1103/PhysRevApplied.2.054007)
11. Cebrecos A, Romero-García V, Picó R, Sánchez-Morcillo VJ, Botey M, Herrero R, Cheng YC, Staliunas K. 2014 Acoustically penetrable sonic crystals based on fluid-like scatterers. *J. Phys. D Appl. Phys.* **48**, 025501. (doi:10.1088/0022-3727/48/2/025501)
12. Aközbek N, Mattiucci N, Bloemer MJ, Sanghadasa M, D'Aguanno G. 2014 Manipulating the extraordinary acoustic transmission through metamaterial-based acoustic band gap structures. *Appl. Phys. Lett.* **104**, 161906. (doi:10.1063/1.4873391)

13. Nicolet A, Zolla F, Geuzaine C. 2010 Transformation optics, generalized cloaking and superlenses. *IEEE Trans. Magn.* **46**, 8.

14. Arslanagic S, Hansen TV, Mortensen NA, Gregersen AH, Sigmund O, Ziolkowski RW, Breinbjerg O. 2013 A review of the scattering-parameter extraction method with clarification of ambiguity issues in relation to metamaterial homogenization. *Antennas Propag. Mag. IEEE* **55**, 2.

15. Castanié A, Mercier JF, Félix S, Maurel A. 2014 Generalized method for retrieving effective parameters of anisotropic metamaterials. *Opt. Express* **22**, 29 937–29 953. (doi:10.1364/OE.22.029937)

16. Oleinik OA, Shamaev AS, Yosifian GA. 1992 *Mathematical problems in elasticity and homogenization*. Amsterdam, The Netherlands: North Holland.

17. Pendry JB, Martín-Moreno L, Garcia-Vidal FJ. 2004 Mimicking surface plasmons with structured surfaces. *Science* **305**, 847–848. (doi:10.1126/science.1098999)

18. Garcia-Vidal FJ, Martín-Moreno L, Pendry JB. 2005 Surfaces with holes in them: new plasmonic metamaterials. *J. Opt. A Pure Appl. Opt.* **7**, 97–101. (doi:10.1088/1464-4258/7/2/013)

19. Kelders L, Allard JF, Lauriks W. 1998 Ultrasonic surface waves above rectangular-groove gratings. *J. Acoust. Soc. Am.* **103**, 5.

20. Maurel A, Félix S, Mercier JF. 2013 Enhanced transmission through gratings: structural and geometrical effects. *Phys. Rev. B* **88**, 115416. (doi:10.1103/PhysRevB.88.115416)

21. Antonakakis T, Craster RV, Guenneau S. 2013 High frequency homogenization of zero-frequency. *New J. Phys.* **15**, 103014. (doi:10.1088/1367-2630/15/10/103014)

22. Bonnet-Bendhia AS, Starling F. 1994 Guided waves by electromagnetic gratings and non-uniqueness examples for the diffraction problem. *Math. Methods Appl. Sci.* **17**, 5.

23. Alù A, D'Aguanno G, Mattiucci N, Bloemer MJ. 2011 Plasmonic Brewster angle: broadband extraordinary transmission through optical gratings. *Phys. Rev. Lett.* **106**, 123902. (doi:10.1103/PhysRevLett.106.123902)

24. Maurel A, Mercier JF, Félix S. 2015 Modal method for the 2D wave propagation in heterogeneous anisotropic media. *JOSA A* **32**, 979–990. (doi:10.1364/JOSAA.32.000979)

25. Nicorovici NA, McPhedran RC, Botten LC. 1995 Photonic band gaps: Noncommuting limits and the acoustic band. *Phys. Rev. Lett.* **75**, 1507. (doi:10.1103/PhysRevLett.75.1507)

26. Movchan AB, Poulton CG, Botten LC, Nicorovici NA, McPhedran RC. 2001 Noncommuting limits in electromagnetic scattering: asymptotic analysis for an array of highly conducting inclusions. *SIAM J. Appl. Math.* **61**, 1706–1730. (doi:10.1137/S0036139999352262)

27. Felbacq D. 2002 Noncommuting limits in homogenization theory of electromagnetic crystals. *J. Math. Phys.* **43**, 52–55. (doi:10.1063/1.1418013)

28. Maurel A, Félix S, Mercier JF. 2013 Enhanced transmission through gratings: structural and geometrical effects. *Phys. Rev. B* **88**, 115416. (doi:10.1103/PhysRevB.88.115416)

29. Cordero ML, Maurel A, Mercier J-F, Félix S, Barra F. 2015 Tuning the wavelength of spoof plasmons by adjusting the impedance contrast in an array of penetrable inclusions. *Appl. Phys. Lett.* **107**, 084104. (doi:10.1063/1.4929497)